Hourly Performance Prediction of Solar Ejector-Absorption Refrigeration Based on Exergy and Exergoeconomic Concept

Fateme Ahmadi Boyaghchi*‡, Reihaneh Taheri*

*Department of Mechanical Engineering, Faculty of Engineering, Alzahra University, Deh Vank, Tehran, Iran

(aboyaghchi@gmail.com, rhn.taheri@gmail.com)

‡Corresponding Author; Department of Mechanical Engineering, Faculty of Engineering, Alzahra University, Deh Vank, Tehran, Iran, Tel: +9821 88044040-2140,

Fax: +9821 88617537, e-mail: aboyaghchi@gmail.com

Received: 17.08.2014 Accepted:28.10.2014

Abstract- Solar cooling technology is being increasingly studied due to its environmental compatibility and cost saving capability. In this article, application of solar absorption refrigeration for cooling of an office building is investigated through modeling and simulation. Solar radiation and cooling load demand have hourly modeled during summer days using Tehran's climate data as a typical weather scenario. The simulation results show that from 9 AM to 5 PM, product cost per exergy unit ($c_{P,tot}$) for the entire system decreases 87%. During this time, thermodynamic coefficient of performance (COP_{th}) increases from 0.16 to 0.48 (auxiliary heat needed reduces fromzz 4.36 to 1.23 kW), suggesting that the performance of the system increases until 5 PM. This is also confirmed by studying exergetic coefficient of performance (COP_{exe}) which reaches to the maximum point at the same time. Furthermore summer days analysis shows that at maximum air temperature the system has optimal *COPs* while the minimum of $c_{P,tot}$ occurs at maximum radiation. The results show the exact times at which the system performs less efficiently by solar energy and therefore the opportunity of using other available renewable energy resources at these times.

Keywords: Solar energy, Absorption refrigeration, Modeling and Simulation, Ammonia-water, Thermoeconomic analysis, Building energy

1. Introduction

Energy crisis and global warming has led to gradual substitution of renewable energy resources for fossil fuels. In recent years, cooling systems based on solar absorption refrigeration has received more attentions. This is because the higher cooling demand is required on days with higher solar radiation [1]. The performance efficiency of solar absorption refrigeration systems has been investigated through thermodynamic modeling and simulation [2, 3]. Also the effect of design conditions on *COP* has been investigated [4]. By considering the weather condition, hourly modeling of solar absorption refrigeration systems has been carried out [5, 6]. The corresponding results show that the performance efficiency of such systems highly depends on solar radiation [5] and air temperature changes [6]. Moreover, hourly modeling is applied to find the best size for the collector and heat storage tank during warm days [7].

An ejector mechanism has been proposed to improve the efficiency of absorption refrigeration systems which shows 20-40% increase for *COP* [8]. Such results have been experimentally studied with 60% improved efficiency [9]. In this context, optimization of *COP* and auxiliary heat has been considered for a solar ejector-absorption refrigeration [10].

To improve cost efficiency along with thermodynamic performance, thermoeconomic modeling and simulation is employed. Thermoeconomic analysis has been carried out to analyze and optimize the product cost and investment cost of

absorption refrigeration systems [11, 12]. In addition, through multi-objective optimization algorithms thermodynamic and thermoeconomic parameters have been optimized simultaneously at the design stage [13, 14]. However to the best of our knowledge, thermoeconomic hourly modeling and simulation of solar absorption refrigeration systems is not studied.

In this study a solar ammonia-water ejector-absorption refrigeration system is modeled and simulated. The application of the system is considered for cooling of an office building that is located in Tehran. Hourly thermodynamic and thermoeconomic analysis of the system is done for different weather conditions of three selected summer days which are June 21st (with maximum insolation), August 6th (with maximum outdoor air temperature) and September 22nd (with minimum insolation and outdoor air temperature). By understanding the system performance during extreme weather conditions, the actual behavior for the entire summer can be predicted. Considering the similar studies in this research area [6, 15], the advantage of this work is thermoeconomic hourly modeling and simulation of solar absorption refrigeration for critical weather conditions in summer days.

2. Modeling

The schematic diagram of an ejector-absorption refrigeration system coupled with a solar collector is illustrated in Fig. 1. In this cycle the evaporator is preparing a chilled water stream that is covering cooling load ($\dot{Q}_{eva}$) of an office building through several fan coils. The cycle contains ammonia refrigerant with constant concentration (x_c) in the evaporator, condenser, ejector and flash tank. The outlet evaporated refrigerant of evaporator gets mixed with water in the absorber and a concentrated solution of ammonia in form of saturated liquid leaves the absorber and after getting warmer enters into the generator. In the generator the saturated vapor of ammonia is extracted and dilute solution returns to the solution heat exchanger. The more purified refrigerant enters to the ejector as the primary fluid and mixes with the secondary fluid coming from the mix chamber. The ejector outlet stream loses heat in the condenser and becomes as a saturated liquid. Cooling processes in both absorber and condenser is done by two closed cooling water streams. In the flash tank, liquid and vapor phases are split in to make more desirable refrigerant. On the other hand, the hot water supplied by an evacuated tube collector enters to the heat storage tank. The outlet hot water from the heat storage tank (point 23) gains more heat from auxiliary heat resource if its temperature is less than generator design temperature and supplies the generator required heat. The working fluid in all stages of the collector and temperature stabilizer subsystems is compressed liquid water.

Computer modeling and simulation has been done in EES software [16] to simulate the performance of this system.

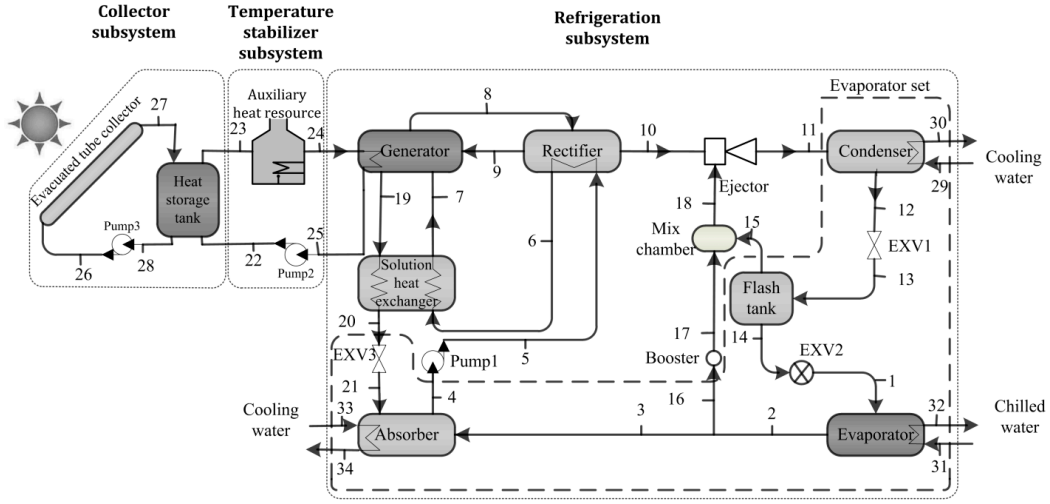

Fig. 1. Schematic diagram of the solar ejector-absorption refrigeration system.

2.1. Thermodynamic modeling

2.1.1.Energy analysis

The process in each component is considered to be steady state and steady flow. Considering each component as a control volume, mass and energy conservation equations are considered [17].

$$\sum_{in} \dot{m}_i = \sum_{out} \dot{m}_o \quad (1)$$

$$\sum_{in} \dot{m}_i x_i = \sum_{out} \dot{m}_o x_o \quad (2)$$

$$\dot{Q} - \dot{W} = \sum_{out} \dot{m}_o h_o - \sum_{in} \dot{m}_i h_i \quad (3)$$

In the above equations, $\dot{m}$ is mass flow rate (kg/s), x is ammonia-water concentration, h is specific enthalpy (kJ/kg), $\dot{Q}$ is heat transfer rate (kW) and $\dot{W}$ is work transfer rate (kW). The inlet primary fluid to the ejector suctions the secondary fluid comes from the mix chamber into the ejector.

The ratio of secondary mass fluid rate to primary mass fluid rate is known as entrainment ratio (ω) which is a function of thermodynamic and physical characteristics of the ejector. In the present modeling the effect of the ejector performance on the entrainment ratio is considered by related relations extracted from [2]. The auxiliary heat is supplied by a boiler which uses natural gas (NG) as fuel and its rate is calculated as [18]:

$$\dot{Q}_{aux} = h_{aux}\dot{m}_{NG}LHV_{NG} \quad (4)$$

where η_{aux} is auxiliary heat resource efficiency and LHV_{NG} is natural gas lower heating value (kJ/kg). By considering the heat storage tank as an intermediate between the collector and the generator, the temperature of heat storage tank T_{hst} is calculated as below [1, 19, 20]: (T_{am} is ambient temperature which is considered as 25°C.)

$$T_{hst,t+1} = T_{hst,t} + \frac{Dt}{(mc_p)_{hst}}[\dot{Q}_{coll} - \dot{Q}_{load} - \dot{Q}_{hstl}] \quad (5)$$

$$\dot{Q}_{coll} = \dot{m}_{27}c_{p,w}(T_{27} - T_{28}) \quad (6)$$

$$\dot{Q}_{load} = \dot{m}_{23}c_{p,w}(T_{23} - T_{22}) \quad (7)$$

$$\dot{Q}_{hstl} = (UA)_{hst}(T_{hst} - T_{am}) \quad (8)$$

where t is time (s), $c_{P,w}$ is specific heat capacity of water (kJ/kg K), mc_P is heat capacity (kJ/K) and UA is loss coefficient cross area of heat storage tank (kW/K). For the evacuated tube collector, $\dot{Q}_{use}$ is considered as useful heat rate gained by water from solar insolation through collector [19].

$$\dot{Q}_{use} = h_{etc}A_aG_t \quad (9)$$

In the above equation A_a is aperture area of collector (m^2) and G_t is the solar insolation rate on the collector tilted surface (kW/m^2) which is described more in section 2.3.1. The efficiency of evacuated tube collector (η_{etc}) is calculated as below [21]:

$$h_{etc} = h_0 - \frac{a_1(T_m - T_{out})}{G_t} - \frac{a_2(T_m - T_{out})^2}{G_t}$$
$$T_m = \frac{T_i + T_o}{2} \quad (10)$$

where T_{out} is outdoor air temperature while T_i and T_o are temperatures of the collector inlet and outlet streams. In this article the coefficient of the above equation are extracted from Apricus Company [22]:

$$h_0 = 0.656, a_1 = 1.4(W/m^2K)$$
$$a_2 = 0.007(W/m^2K^2) \quad (11)$$

2.1.2. Exergy analysis

Exergy is mainly consists of physical and chemical exergies. Physical exergy is defined as the maximum work is done by a system to transfer from the state with certain temperature and pressure to the reference environment state (which is denoted by *0* in the following equations). Chemical exergy is the maximum work is done to transfer from reference environment to dead state. By considering specific enthalpy h and specific entropy s (kJ/kg), the specific physical exergy is defined as [18]:

$$ex^{PH} = (h - h_0) - T_0(s - s_0) \quad (12)$$

In this article the liquid water at 25°C and 101.325 kPa is assumed to be as the reference environment. Chemical exergy of water in the collector and temperature stabilizer subsystems is neglected and specific chemical exergy of ammonia-water solution is calculated as below [23]:

$$ex^{CH}_{Sol} = [\frac{\overline{ex}^0_{CH,NH_3}}{M_{NH_3}}]x + [\frac{\overline{ex}^0_{CH,H_2O}}{M_{H_2O}}](1 - x) \quad (13)$$

where M is molar mass (kg/kmol) and $\overline{ex}^0_{CH}$ is standard molar chemical exergy which its value for ammonia (NH_3) and water (H_2O) is extracted from references [18, 24].

In this study the Fule-Product Method has been applied for exergy analysis. Fuel exergy rate ($\dot{X}_F$) and product exergy rate ($\dot{X}_P$) are defined as required input and desired output, respectively. The inefficiencies are measured by exergy loss rate ($\dot{X}_L$) and exergy destruction rate ($\dot{X}_D$). If the heat transfer process happens at constant temperature for a component (T_k), the exergy loss is given by [18]:

$$\dot{X}_L = (1 - \frac{T_0}{T_k})\dot{Q}_k \quad (14)$$

The exergy destruction ($\dot{X}_D$), exergetic efficiency (η_{exe}), exergy destruction ratios (y_D , y_D^*) and exergy loss ratio (y_L) are also calculated for the exergy analysis as following [18]:

$$\dot{X}_D = \dot{X}_F - \dot{X}_P - \dot{X}_L \quad (15)$$

$$h_{exe} = \frac{\dot{X}_P}{\dot{X}_F} = 1 - \frac{\dot{X}_D + \dot{X}_L}{\dot{X}_F} \quad (16)$$

$$y_D = \frac{\dot{X}_D}{\dot{X}_{F,tot}}, y_D^* = \frac{\dot{X}_D}{\dot{X}_{D,tot}} \quad (17)$$

$$y_L = \frac{\dot{X}_L}{\dot{X}_{F,tot}} \quad (18)$$

A proper 'Fuel-Product-Loss' definition for each component of the system is necessary for an efficient exergy analysis to describe the actual nature of physical flows. In the refrigeration subsystem determining fuel and product roles is easy for the evaporator, solution heat exchanger, generator, rectifier, mix chamber and pumps where exergy of the product is increased. On the other hand, for the absorber, condenser, flash tank and expansion valves special considerations are applied because of complicity of product defining. By considering Bejan et al. [18] method a single

virtual component is considered as a representative of these components and is shown as evaporator set. Appling mentioned assumptions and related formulas presented in references [18, 23, 25], F-P-L definition of components are represented in Table 1.

The exergy loss of heat storage tank ($\dot{X}_{hstl}$) is calculated by equation (14) and the exergy rate of heat supplied by auxiliary heat resource is calculated as below [18]:

$$\dot{X}_{NG} = \dot{m}_{NG} R_{NG} T_0 \ln(\frac{P_{NG}}{P_0}) + \dot{m}_{NG} \frac{\overline{ex}^{0}_{CH,NG}}{M_{NG}} \quad (19)$$

where R_{NG} is individual gas constant (KJ/kg K), P_{NG} is pressure (kPa) and M_{NG} is molar mass of natural gas. Also the input solar exergy is considered as following while T_{sun} is assumed to be 6000 K [26]:

$$\dot{X}_{sun} = G_t A_a (1 + \frac{1}{3}(\frac{T_0}{T_{sun}})^4 - \frac{4}{3}(\frac{T_0}{T_{sun}})) \quad (20)$$

Thermodynamic coefficient of performance (COP_{th}) is considered for the system as the ratio of the energy extracted from chilled water through the evaporator to the total energy supplied to the system [12].

$$COP_{th} = \frac{\dot{Q}_{eva}}{A_a G_t + \dot{m}_{NG} LHV_{NG} + \sum_{pmp1,2,3,bst} \dot{W}} \quad (21)$$

Considering same conception, exergetic coefficient of performance (COP_{exe}) is defined as:

$$COP_{exe} = \frac{\dot{X}_{32} - \dot{X}_{31}}{\dot{X}_{sun} + \dot{X}_{NG} + \sum_{pmp1,2,3,bst} \dot{W}} \quad (22)$$

2.1.3. Thermoeconomic modeling

Cost balance for each component indicates that the sum of cost rates associated with all exiting streams equals the sum of cost rates of all entering streams plus capital investment, operating and maintenance (O&M) cost rates. Considering heat is received (denoted by q subscript) and work is produced by a component (denoted by w subscript) the cost balance equation would be [18]:

$$\sum_{out} c_o \dot{X}_o + c_w \dot{X}_w = c_q \dot{X}_q + \sum_{in} c_i \dot{X}_i + \dot{Z}$$
$$\dot{Z} = \frac{Z^{CI} + Z^{OM}}{ta} \quad (23)$$

Table 1. Definition of fuel exergy, product exergy and exergy loss of the solar ejector-absorption refrigeration system components

Name	$\dot{X}_F$	$\dot{X}_P$	$\dot{X}_L$
Evaporator set	$\dot{X}_{11} - \dot{X}_{15} - \dot{X}_{16} + \dot{X}_{20} - \dot{X}_4$	$\dot{X}_{32} - \dot{X}_{31}$	$\dot{X}_{30} - \dot{X}_{29} + \dot{X}_{34} - \dot{X}_{33}$
Solution heat exchanger	$\dot{X}_{19} - \dot{X}_{20}$	$\dot{X}_7 - \dot{X}_6$	0
Generator	$\dot{X}_{24} - \dot{X}_{25}$	$\dot{X}_8 - \dot{X}_7 + \dot{X}_{19} - \dot{X}_9$	0
Rectifier	$\dot{X}_8 - \dot{X}_{10} - \dot{X}_9$	$\dot{X}_6 - \dot{X}_5$	0
Ejector	$\dot{X}_{10} + \dot{X}_{18}$	$\dot{X}_{11}$	0
Booster	$\dot{W}_{bst}$	$\dot{X}_{17} - \dot{X}_{16}$	0
Mix chamber	$\dot{X}_{15} + \dot{X}_{17}$	$\dot{X}_{18}$	0
Auxiliary heat resource	$\dot{X}_{NG}$	$\dot{X}_{24} - \dot{X}_{23}$	0
Heat storage tank	$\dot{X}_{27} + \dot{X}_{22}$	$\dot{X}_{23} + \dot{X}_{28}$	$\dot{X}_{hstl}$
Evacuated tube collector	$\dot{X}_{sun}$	$\dot{X}_{27} - \dot{X}_{26}$	0
Pump	$\dot{W}_{pmp}$	$\dot{X}_o - \dot{X}_i$	0

Where c is cost per exergy (\$/kJ), $\dot{X}$ is exergy rate (kJ/s), Z^{CI} is annual capital investment cost (\$), Z^{OM} is annual operating and maintenance cost (\$) and ta is annual time of operation (s). By considering the above equations for all components and auxiliary relations from references [18, 23, 27, 28] cost per exergy unit of all streams can be obtained. The cost rate of exergy loss is calculated by equation (24) and the capital investment and O&M cost rates is calculated by a procedure explained in Appendix A. Therefore by considering the cost balance as equation (25) product, fuel

and loss cost rates ($\dot{C}_P, \dot{C}_F$ and $\dot{C}_L$) for all components are revealed [18]:

$$\dot{C}_L = c_F \dot{X}_L, (\dot{X}_P = cte) \quad (24)$$

$$\dot{C}_P = \dot{C}_F - \dot{C}_L + \dot{Z} \quad (25)$$

Thermoeconomic evaluation is done by means of five important thermoeconomic variables which are namely; cost per exergy unit of fuel (c_F), cost per exergy unit of product (c_P), cost rate of exergy destruction ($\dot{C}_D$), relative cost difference (r) and exergoeconomic factor (f) which are calculated as below [18]:

$$c_F = \frac{\dot{C}_F}{\dot{X}_F} \quad (26)$$

$$c_P = \frac{\dot{C}_P}{\dot{X}_P} \quad (27)$$

$$\dot{C}_D = c_F \dot{X}_D, (\dot{X}_P = cte) \quad (28)$$

$$r = \frac{c_P - c_F}{c_F} \quad (29)$$

$$f = \frac{\dot{Z}}{\dot{Z} + c_F (\dot{X}_D + \dot{X}_L)} \quad (30)$$

The cost per exergy unit of product can be considered for the overall system as following:

$$c_{P,tot} = \frac{\dot{C}_{32} - \dot{C}_{31}}{\dot{X}_{32} - \dot{X}_{31}} \quad (31)$$

2.2. Hourly climate data

2.2.2. Solar insolation

Necessary equations for calculating the solar insolation on the collector tilted surface G_t are taken from [1]. G_t is calculated through total insolation on horizontal surface G and diffuse insolation on horizontal surface G_D as below:

$$\frac{G_t}{G} = (1 - \frac{G_D}{G}) R_B + \frac{G_D}{G} (\frac{1 + \cos(b_c)}{2}) + r_G (\frac{1 - \cos(b_c)}{2}) \quad (32)$$

$$R_B = \frac{\sin(L - b_c)\sin(d) + \cos(L - b_c)\cos(d)\cos(h)}{\sin(L)\sin(d) + \cos(L)\cos(d)\cos(h)} \quad (33)$$

where L is latitude (degree), δ is declination (degree), β_c is incident angle of the collector (degree), ρ_G is ground reflectance albedo and h is hour angle (degree). Daily total insolation incident on a horizontal surface H and daily average insolation clearness index $\bar{K}_T$ are available for Tehran coordinates from [29]. To extract the hourly values, the ratio of hourly total insolation to daily total insolation r is calculated: (h_{ss} is sunset hour angle in degree)

$$r = \frac{p}{24}[a + b\cos(h)] \frac{\cos(h) - \cos(h_{ss})}{\sin(h_{ss}) - (\frac{2\pi h_{ss}}{360})\cos(h_{ss})} \quad (34)$$

$$a = 0.409 + 0.5016 \sin(h_{ss} - 60)$$
$$b = 0.6609 - 0.4767 \sin(h_{ss} - 60)$$

Also by considering daily diffuse insolation H_D, the ratio of hourly diffuse insolation to daily diffuse insolation r_D is calculated:

$$\frac{H_D}{H} = 1.390 - 4.027\bar{K}_T + 5.531\bar{K}_T^2 - 3.108\bar{K}_T^3 \quad (35)$$

$$r_D = (\frac{p}{24}) \frac{\cos(h) - \cos(h_{ss})}{\sin(h_{ss}) - (\frac{2\pi h_{ss}}{360})\cos(h_{ss})} \quad (36)$$

2.2.3. Cooling load

The Radiant time series method [30] is applied to calculate the hourly cooling load of a floor office in Tehran with 81 m^2 floor area, 4 south face windows and 10 occupants working from 9 AM to 5 PM. Cooling load is defined as the rate at which the energy should be sent out from the space to keep the space temperature and humidity at constant design values. Cooling load is strongly dependent to solar insolation and outdoor air temperature.

Considering weather data and the simulation results, during a day the approximately same variation of hourly outdoor air temperature and solar insolation on tilted collector surface happen. This can be seen in Fig. 2 for three summer days which are June 21st August 6th and September 22nd with different weather conditions. The maximum value of the insolation on the collector surface is 969 W/m^2 at 13 o'clock on June 21st and The maximum value of outdoor air temperature is 36.88°C at 15 o'clock on August 6th. Also the minimum insolation and temperature values can be seen for September 22nd.

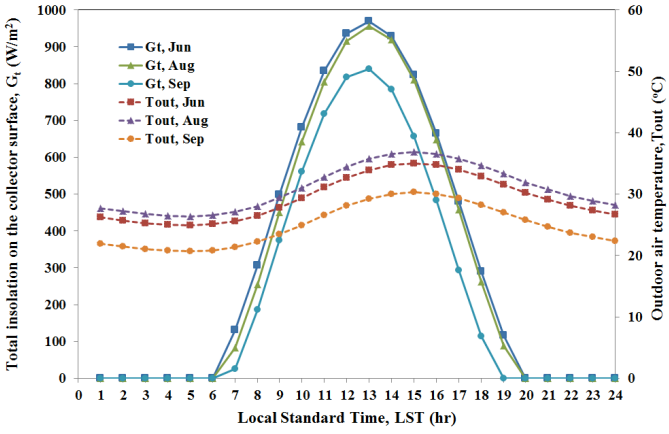

Fig. 2. Hourly variation of insolation on tilted collector surface and outdoor air temperature during summer (β_c=13°).

2.3. Validation

For validation the results calculated by the model of present study are compared with the experimental values extracted from Abdulateef et al. [31] work. For different generator and evaporator temperature, thermal *COP* is calculated and compared to the corresponding results from the experimental work. According to the values of Normalized Root Mean Square Error (NRMSE) which is used to measure the difference, the results of present study are found to be in good agreement with experimental values with error no more than 16%. This shows enough reliability for the model to analyze the performance of the solar ammonia-water ejector-absorption refrigeration system.

3. Results and discussion

Table 3 and Table 4 represent the results of respectively exergy and thermoeconomic analysis of the system components for the weather condition appears at 13 o'clock on 6st of August and under the design conditions explained in Table 2.

Table 2. Design conditions assumed for the solar ejector-absorption refrigeration system

Variable name	Symbol	Value
Evaporator temperature	T_{eva}	10 °C
Generator temperature	T_{gen}	85 °C
Generator pressure	P_{gen}	1800 kPa
Ammonia concentration	Xc	0.9996

According to the results shown in Table 3 the maximum exergy loss rate of 0.11 kW belongs to the evaporator set with y_L of 0.476%. The collector has the highest amount of exergy destruction rate of 18.45 kW with y_D^* of 82.36%. The high value of exergy destruction in the collector is because of irreversibility due to fuel and product exergy difference which also leads to low exergy efficiency of 8.41%. After the collector, the auxiliary heat resource and heat storage tank have more exergy destruction than other components.

Table 3. Exergy analysis results of the solar ejector-absorption refrigeration system

Name	$\dot{X}_F$ (kW)	$\dot{X}_P$ (kW)	$\dot{X}_D$ (kW)	$\dot{X}_L$ (kW)	y_D (%)	y_D^* (%)	y_L (%)	η_{exe} (%)
Evaporator set	1.03	0.08	0.84	0.10790	3.707	3.749	0.476	7.67
Solution heat exchanger	0.26	0.13	0.13	0	0.591	0.598	0	48.48
Generator	1.38	1.31	0.07	0	0.294	0.297	0	95.18
Rectifier	0.08	0.02	0.06	0	0.283	0.286	0	19.10
Ejector	1.42	1.28	0.14	0	0.607	0.614	0	90.32
Booster	0.01	0.01	0.00	0	0.001	0.001	0	99.01
Mix chamber	0.11	0.11	0.00	0	0.002	0.002	0	99.60
Auxiliary heat resource	2.45	0.37	2.09	0	9.210	9.315	0	14.92
Heat storage tank	5.10	3.64	1.40	0.06814	6.160	6.230	0.301	71.31
Evacuated tube collector	20.14	1.69	18.45	0	81.430	82.360	0	8.41
pumps	0.05	0.04	0.00	0	0.02	0.02	0	90.91

The results on Table 4 shows that the heat storage tank and evaporator set have the highest values of $\dot{Z} + \dot{C}_D + \dot{C}_L$ and also low values for f which means their important thermoeconomic role is highly associated with exergy destruction. By reducing heat loss in the heat storage tank and increasing evaporator design temperature, exergy destructions can be avoided. About 48% of capital investment and O&M costs rate of the whole system are allocated to the evacuated tube collector.

The relative cost difference of the collector is obtained infinity because the fuel cost of the collector is assumed to be zero. Product cost per exergy unit of the solution heat exchanger and auxiliary heat resource are highest and lowest respectively among all components. In this study the hourly analysis of three important days during summer are discussed: June 21st, August 6th and 22nd of September. As the weather condition changes by time, the system meets various cooling loads and collector heat gains.

Hourly and daily analysis of solar refrigeration systems is critical for evaluating their efficiency. By considering the system operation time from 9 AM to 5 PM adjusted to working hours and the design conditions for the system, the hourly analysis results are illustrated in Fig. 3-7.

The hourly variation of heat transfer rates are plotted in Fig. 3. The useful insolation heat gained by the collector ($\dot{Q}_{use}$) has the same trend as solar insolation. According to the average value of three days the evaporator heat transfer rate ($\dot{Q}_{eva}$) or cooling load increases about 70% during the working hours while the generator heat transfer rate follows that by same rate. Although the solar insolation decreases at afternoon, the cooling load is still increasing due to high value of outdoor air temperature. On the other hand, the

auxiliary heat transfer rate ($\dot{Q}_{aux}$) decreases about 70% during the working hours. Since at early hours of the day the temperature of heat storage tank is much lower than the temperature of hot water required for generator, auxiliary heat resource supplies more amount of the generator required heat than the heat storage tank.

Table 4. Thermoeconomic results of the solar ejector-absorption refrigeration system

Name	c_F ($/MJ)	c_P ($/MJ)	$\dot{C}_D$ ($/Year)	$\dot{C}_L$ ($/Year)	$\dot{Z}$ ($/Year)	$\dot{Z}+\dot{C}_D+\dot{C}_L$ ($/Year)	f	r
Evaporator set	2.519	3.748	6094.08	782.78	689.76	7566.62	0.09	0.49
Solution heat exchanger	3.169	6.707	1222.56	0	61.75	1284.31	0.05	1.12
Generator	1.796	1.907	344.16	0	78.16	422.32	0.19	0.06
Rectifier	0.450	3.035	82.92	0	29.72	112.64	0.26	5.75
Ejector	2.147	2.377	849.89	0	0.00	849.89	0.00	0.11
Booster	0.012	1.994	0.00	0	75.46	75.46	1.00	166.00
Mix chamber	2.364	2.373	3.10	0	0.00	3.10	0.00	0.00
Auxiliary heat resource	0.004	0.413	25.66	0	396.00	421.66	0.94	95.79
Heat storage tank	2.629	3.728	10566.72	515.81	950.69	12033.22	0.08	0.42
Evacuated tube collector	0	0.452	0	0	2204.06	2204.06	1.00	infinity
pumps	0.036	4.458	0.15	0	119.12	119.27	1.00	123.45

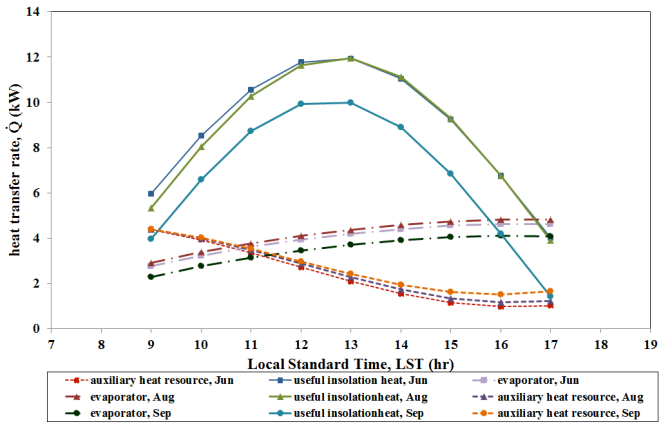

Fig. 3. Variation of heat transfer rates of the evaporator and auxiliary heat resource and useful insolation gained by the collector during summer.

So, the most amount of $\dot{Q}_{use}$ is consumed to increase the temperature of heat storage tank which causes considerable decrease in amount of $\dot{Q}_{aux}$ by time. At the end of a day $\dot{Q}_{aux}$ increases again to cover the lack of solar insolation. Comparison of results of summer days show that on June 21st the collector receives the highest insolation with the average of 8.87 kW, while the cooling load is not as much as cooling load of the warmest day in August. Consequently, the auxiliary heat for June 21st with the average of 2.35 kW is less than other days. By way of contrast, despite appearing the minimum cooling load on September 22nd the auxiliary heat of this day is the maximum among other days due to low amount of received insolation.

According to Fig. 4, the amount of COP_{th} and COP_{exe} increases with the average of about 136% and 316% respectively during working hours with rapid growth from 13 to 17 due to cooling load increase and insolation and auxiliary heat decrease simultaneously. Generally, the highest values of COP_{th} and COP_{exe} happen on August and the lower values happen at respectively June and September. Therefore, the system is more efficient in the middle of summer. Also daily increase of COP_{th} and COP_{exe} of September 22nd is more than other days obviously after 13 O'clock because it gets cold and dark sooner on the end days of summer.

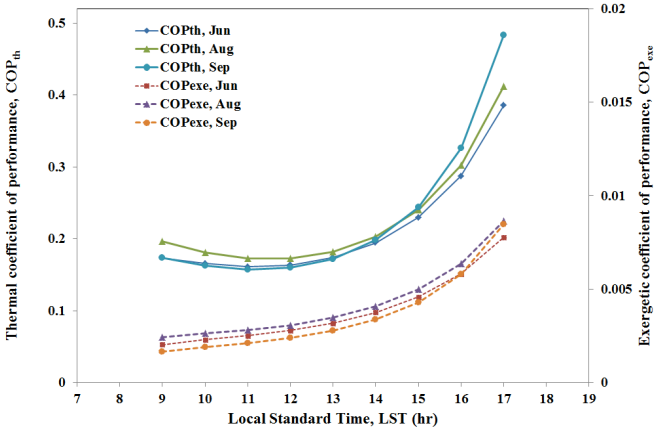

Fig. 4. Variation of thermal and exergetic coefficient of performance during summer.

In Fig. 5 total exergy destruction rate increases with the average of 42% until 12 o'clock and decreases with the average of 55% from 12 to 17 O'clock obviously following the insolation trend. Also the exergy destruction rate of the evaporator set increases with the average of 56% during the day due to ascending trend of cooling load. Total exergy destruction rate of June 21st is higher than other days while September 22nd has the lowest one. The main reason is that total exergy destruction is mostly dependent to solar

insolation which has the maximum value for June. On the other hand, the maximum values of exergy destruction rate of the evaporator set belongs to August 6th with the average of 0.80 kW due to high amount of cooling load for this day.

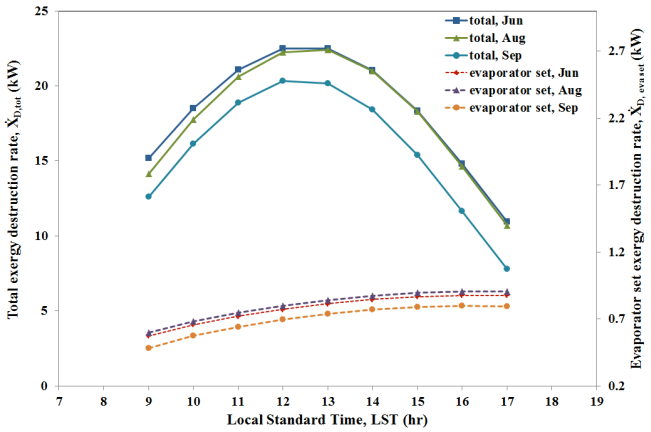

Fig. 5. Variation of exergy destruction rate of the evaporator set and whole system during summer.

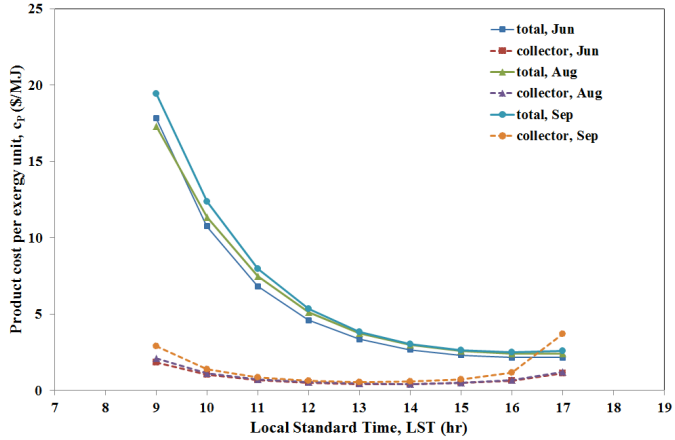

Fig. 6. Variation of product cost per exergy unit of the evacuated tube collector and whole system during summer.

According to Fig. 6, the product cost per exergy unit of the whole system ($c_{P,tot}$) decreases with the average of 87% due to increase in cooling load. Because of solar insolation changes, the collector product cost per exergy unit decreases from morning to reach to the average of 0.48 $/MJ at 13 O'clock and increases again. It means for more values of solar insolation the collector product costs less. Generally, product cost per exergy unit of the collector and whole system for September 22nd is about 1.5 times as much as other days because of less amount of insolation in this day. On the other hand, the minimum values of product cost per exergy unit of the collector and whole system are allocated to 21st of June.

The cost rates of exergy destruction and exergy loss for evaporator set are plotted in Fig. 7. The figure shows that they both increase during summer days while cost rate of exergy destruction increases 40% which is about 1/4th of cost rate of exergy loss increase. Also cost rates of exergy destruction and loss for August 6th is the maximum among other days due to more related values of exergy destruction for this day shown in Fig. 5.

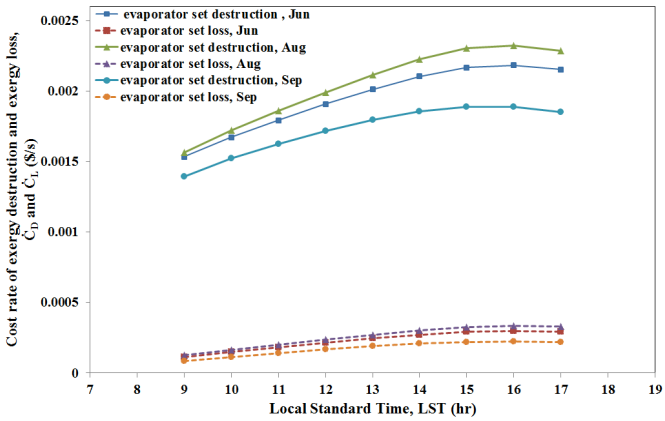

Fig. 7. Variation of cost rate of exergy destruction and exergy loss of the evaporator set during summer.

4. Conclusion

Thermodynamic and thermoeconomic modeling of a solar ejector-absorption refrigeration system used for cooling of an office building was presented. Simulation of the model for three summer days with different weather conditions was performed. From the simulation results, the outcomes are obtained:

- According to the hourly analysis, from 9 AM to 5 PM, cooling load increases about 70%, which is owing to high value of outdoor air temperature at afternoon, while the auxiliary heat transfer rate decreases by same rate. This decrement is due to increment of the internal energy of storage tank. The minimum amount of auxiliary heat transfer rate happens on June 21st and the maximum on September 22nd.
- During a day, COP_{th} and COP_{exe} increase about 136% and 316% while $c_{P,tot}$ decreases 87%. The maximum *COPs* and minimum $c_{P,tot}$ happen on August 6th and June 21st respectively, while the minimum *COPs* and maximum $c_{P,tot}$ take place on September 22nd simultaneously.
- During a day by increasing solar insolation, total exergy destruction rate increases with highest values for June 21st. The exergy destruction rate and exergy destruction cost rate of the evaporator set increase about 56% and 40% respectively where August 6th has the higher values for them.

Generally, the hourly results show that at the late hours of a summer day the system performs more efficient in terms of thermodynamic, exergy and product cost. The monthly results indicate that during the summer season, a supplementary energy resource becomes more critical towards the later of the summer. The system is more performance efficient in the middle of summer and it is more cost efficient in the beginning of summer.

Appendix A

To calculate *TCI* the capital investment cost ($) of a component at a specific size or capacity from reference available cost (denoted by *R* subscript), following relations are used for a heat exchanger and a pump [11, 13]:

$$TCI_{hex} = TCI_{R,hex}(\frac{A_{hex}}{A_{R,hex}})^{0.6} \quad (37)$$

$$A_{hex} = \frac{\dot{Q}_{hex}}{U_{hex} \times LMTD_{hex}} \quad (38)$$

$$TCI_{pmp} = TCI_{R,pmp}(\frac{\dot{W}_{pmp}}{\dot{W}_{R,pmp}})^{0.26}(\frac{1-h_{pmp}}{h_{pmp}})^{0.5} \quad (39)$$

where A_{hex} is area (m^2), $\dot{Q}_{hex}$ is heat transfer rate (kW), U_{hex} is overall heat transfer coefficient (kW/ m^2 K) and *LMTD* is logarithmic mean temperature difference of heat exchanger. Pump power and pump efficiency are also illustrated by $\dot{W}_{pmp}$ and η_{pmp} respectively. For the evaporator, absorber, solution heat exchanger, rectifier and condenser which are considered as heat exchanger the reference costs are available at references [11, 32] and the value of U_{hex} is extracted from literature [27, 32]. The capital investment costs of the ejector, flash tank, mix chamber and expansion valves are neglected due to their small amount in compare to others [14, 27]. The capital investment costs of the components of the collector and temperature stabilizer subsystems are extracted form Apricus Company [22]. The annual capital investment cost is calculated through capital recovery factor *CRF* which is defined by interest rate *i* and life time of the system in years *N* that are assumed 0.15 and 20 years respectively in this work [18]:

$$Z^{CI} = CRF \times TCI, CRF = \frac{i(1+i)^N}{(1+i)^N - 1} \quad (40)$$

Annual operating and maintenance (O&M) cost consists of the cost related to capital investment, the cost related to product exergy rate and all other O&M costs (γ_0) [18].

$$Z^{OM} = g_2(TCI) + g_1 t_a \dot{X}_P + g_0 \quad (41)$$

In this study the contribution of the capital investment cost is considered more than others. As a result γ_2 is assumed to be 1.25% and other terms are neglected [12, 13, 23]. The price of electricity used by pumps and the price of natural gas used by auxiliary heat resource is considered 0.043 \$/kWh and 0.040 \$/m^3 respectively due to prices offered by Iranian energy companies.

All cost data used in an economic analysis at different years (Cd_O) must be brought to the base year 2013 (Cd_B) through cost indexes ($CIndex_B$ and $CIndex_O$) extracted from Chemical engineering plant Cost Index [18, 33]:

$$Cd_B = Cd_O \times \frac{CIndex_B}{CIndex_O} \quad (42)$$

References

[1] S. A. Kalogirou, Solar Energy Engineering: Processes and Systems: Elsevier Science, 2009.

[2] D. W. Sun, I. W. Eames, and S. Aphornratana, "Evaluation of a novel combined ejector-absorption refrigeration cycle - I: computer simulation," International Journal of Refrigeration, vol. 19, pp. 172-180, 1996.

[3] S. G. Alvares and C. Trepp, "Simulation of a solar driven aqua-ammonia absorption refrigeration system Part 1: mathematical description and system optimization," International Journal of Refrigeration, vol. 10, pp. 40-48, 1987.

[4] N. K. Ghaddar, M. Shihab, and F. Bdeir, "Modeling and simulation of solar absorption system performance in Beirut," Renewable Energy, vol. 10, pp. 539-558, 1997.

[5] I. Atmaca and A. Yigit, "Simulation of solar-powered absorption cooling system," Renewable Energy, vol. 28, pp. 1277-1293, 2003.

[6] M. Mazloumi, M. Naghashzadegan, and K. Javaherdeh, "Simulation of solar lithium bromide–water absorption cooling system with parabolic trough collector," Energy Conversion and Management, vol. 49, pp. 2820-2832, 2008.

[7] M. Ozgoren, M. Bilgili, and O. Babayigit, "Hourly performance prediction of ammonia–water solar absorption refrigeration," Applied Thermal Engineering, vol. 40, pp. 80-90, 2012.

[8] F. Assilzadeh, S. A. Kalogirou, Y. Ali, and K. Sopian, "Simulation and optimization of a LiBr solar absorption cooling system with evacuated tube collectors," Renewable Energy, vol. 30, pp. 1143-1159, 2005.

[9] A. Sözen and M. Özalp, "Solar-driven ejector-absorption cooling system," Applied Energy, vol. 80, pp. 97-113, 2005.

[10] S. Aphornratana and I. W. Eames, "Experimental investigation of a combined ejector-absorption refrigerator: Aphornratana, S. and Eames, I. W. Int. J. Energy Res., 1998, 22, (3), 195–207," Fuel and Energy Abstracts, vol. 39, p. 305, 1998.

[11] L. Garousi Farshi, S. M. S. Mahmoudi, and M. A. Rosen, "Exergoeconomic comparison of double effect and combined ejector-double effect absorption refrigeration systems," Applied Energy, vol. 103, pp. 700-711, 2013.

[12] R. D. Misra, P. K. Sahoo, S. Sahoo, and A. Gupta, "Thermoeconomic optimization of a single effect water/LiBr vapour absorption refrigeration system," International Journal of Refrigeration, vol. 26, pp. 158-169, 2003.

[13] V. Zare, S. M. S. Mahmoudi, M. Yari, and M. Amidpour, "Thermoeconomic analysis and optimization of an ammonia–water power/cooling cogeneration cycle," Energy, vol. 47, pp. 271-283, 2012.

[14] B. H. Gebreslassie, G. Guillén-Gosálbez, L. Jiménez, and D. Boer, "Design of environmentally conscious absorption cooling systems via multi-objective optimization and life cycle assessment," Applied Energy, vol. 86, pp. 1712-1722, 2009.

[15] R. Sirwan, M. A. Alghoul, K. Sopian, and Y. Ali, "Thermodynamic analysis of an ejector-flash tank-absorption cooling system," Applied Thermal Engineering, vol. 58, pp. 85-97, 2013.

[16] S. Klein and F. Alvarado. Engineering equation solver. Http://Www.Fchart.Com

[17] Y. A. Çengel and M. A. Boles, Thermodynamics: an engineering approach: McGraw-Hill Higher Education, 2006.

[18] A. Bejan, G. Tsatsaronis, and M. J. Moran, Thermal Design and Optimization: Wiley, 1996.

[19] L. J. He, L. M. Tang, and G. M. Chen, "Performance prediction of refrigerant-DMF solutions in a single-stage solar-powered absorption refrigeration system at low generating temperatures," Solar Energy, vol. 83, pp. 2029-2038, 2009.

[20] M. Wang, J. Wang, Y. Zhao, P. Zhao, and Y. Dai, "Thermodynamic analysis and optimization of a solar-driven regenerative organic Rankine cycle (ORC) based on flat-plate solar collectors," Applied Thermal Engineering, vol. 50, pp. 816-825, 2013.

[21] A. Pongtornkulpanich, S. Thepa, M. Amornkitbamrung, and C. Butcher, "Experience with fully operational solar-driven 10-ton LiBr/H2O single-effect absorption cooling system in Thailand," Renewable Energy, vol. 33, pp. 943-949, 2008.

[22] http://www.Apricus.Com.Au product specification sheet. (2013).

[23] R. D. Misra, P. K. Sahoo, and A. Gupta, "Thermoeconomic evaluation and optimization of an aqua-ammonia vapour-absorption refrigeration system," International Journal of Refrigeration, vol. 29, pp. 47-59, 2006.

[24] T. J. Kotas, The Exergy Method of Thermal Plant Analysis: Krieger Publishing Company, 1995.

[25] C. A. Frangopoulos and U. Staff, Exergy, Energy System Analysis and Optimization: EOLSS Publishers Company Limited, 2009.

[26] F. A. Al-Sulaiman, I. Dincer, and F. Hamdullahpur, "Exergy modeling of a new solar driven trigeneration system," Solar Energy, vol. 85, pp. 2228-2243, 2011.

[27] V. Zare, S. M. S. Mahmoudi, and M. Yari, "An exergoeconomic investigation of waste heat recovery from the Gas Turbine-Modular Helium Reactor (GT-MHR) employing an ammonia–water power/cooling cycle," Energy, vol. 61, pp. 397-409, 2013.

[28] F. Kreith, CRC Handbook of Thermal Engineering: Taylor & Francis, 2000.

[29] Https://eosweb.larc.nasa.gov. (2013).

[30] F. C. McQuiston, J. D. Parker, and J. D. Spitler, Heating, ventilating, and air conditioning: analysis and design: John Wiley & Sons, 2005.

[31] J. Abdulateef, M. Alghoul, A. Zaharim, and K. Sopian, "Experimental Investigation on Solar Absorption Refrigeration System in Malaysia," in Proceedings of the 3rd Wseas Int. Conf. On Renewable Energy Sources, 2009, pp. 1-3.

[32] B. H. Gebreslassie, G. Guillén-Gosálbez, L. Jiménez, and D. Boer, "Solar assisted absorption cooling cycles for reduction of global warming: A multi-objective optimization approach," Solar Energy, vol. 86, pp. 2083-2094, 2012.

[33] "Economic Indicators, Chemical engineering plant Cost Index (CEPCI)," Chemical engineering, September 2013.